Weierstraß-Institut
für Angewandte Analysis und Stochastik

im Forschungsverbund Berlin e.V.

Preprint ISSN 0946 – 8633

On a thermomechanical milling model

Krzysztof Chełminski[1], Dietmar Hömberg[2], Oliver Rott[2]

submitted: September 15, 2008

[1] Warsaw University of Technology
Faculty of Mathematics
and Information Science
pl. Politechniki 1
00-661 Warsaw
Poland
E-Mail: kchelmin@mini.pw.edu.pl

[2] Weierstrass Institute
for Applied Analysis
and Stochastics
Mohrenstr. 39
10117 Berlin
Germany
E-Mail: hoemberg@wias-berlin.de
rott@wias-berlin.de

No. 1361
Berlin 2008

2000 *Mathematics Subject Classification.* 74F05, 35Q80, 35L15.

Key words and phrases. Thermo-elasticity, milling, process-structure interaction, work piece effects, stability, delay-differential equations.

This work has been supported by the DFG SPP 1180. The first author was partially supported by polish government grant: KBN 1-P03A-031-27.

Edited by
Weierstraß-Institut für Angewandte Analysis und Stochastik (WIAS)
Mohrenstraße 39
10117 Berlin
Germany

Fax: + 49 30 2044975
E-Mail: preprint@wias-berlin.de
World Wide Web: http://www.wias-berlin.de/

Abstract

This paper deals with a new mathematical model to characterize the interaction between machine and workpiece in a milling process. The model consists of a harmonic oscillator equation for the dynamics of the cutter and a linear thermoelastic workpiece model. The coupling through the cutting force adds delay terms and further nonlinear effects. After a short derivation of the governing equations it is shown that the complete system admits a unique weak solution. A numerical solution strategy is outlined and complemented by numerical simulations of stable and unstable cutting conditions.

1 Introduction

A milling machine is a machine tool for the shaping of metal or other solids. Its basic components are a rotating cutter and a table on which the workpiece is mounted. The modelling of milling dynamics, the determination of stable cutting conditions and the design of more efficient milling machines are important research fields in production technology. Effective methods to predict stable processes have been developed in recent years (cf. Altintas et al. [2], Faassen [5]).

An essential part of these methods is an abstract dynamical model, represented by an ordinary differential equation. Adjusted to vibration measurement data it reproduces local characteristics of the actual milling system in terms of the dynamics at the tip of the cutter. Its combination with a process model to describe the cutting forces leads to a delay-differential equation (DDE). The last decade has seen a number of approaches to identify efficiently stable machining parameters by means of bifurcation analysis of these DDE systems (cf., e.g., Faassen [5], Insperger [9]).

However, these methods provide only few detailed information about the dynamics of the entire process. Therefore the focus of this paper is the derivation of an improved model allowing for the inclusion of workpiece effects. In addition to the DDE model for the cutter the workpiece is accounted for by a thermoelastic material model. The coupling is realised through the cutting force. This approach allows for a refined stability analysis and will eventually lead an improved theoretical derivation of stable cutting conditions.

The paper is organised as follows: In Section 2 we derive the model equations. Section 3 is devoted to a mathematical analysis of the resulting system of equations in the case of vanishing feed velocity. In that case we are able to prove the existence of a unique weak solution to a slightly regularised model. An algorithm for the numerical approximation of the new milling model is outlined in Section 4. Particular attention is paid to the changing workpiece geometry in the case of non-zero feeding velocity. Numerical results for different scenarios corresponding to stable and unstable cutting conditions are included. The last section is devoted to some concluding remarks.

2 Modelling

2.1 Preliminaries

Figure 1 shows the principal components of the milling model to be developed. Typically, the influence of the machine on the cutter tip dynamics is described as a multibody system accounting for the many different construction components in terms of rigid bodies coupled through springs and dashpots. Since the focus of our investigations lies in the interplay between machine and workpiece dynamics, it is sufficient to model the cutter as a point mass that may vibrate in x, y-plane.

The workpiece is assumed to behave like a thermo-elastic continuum. We denote the workpiece domain with $\Omega(t) \subset \mathbb{R}^3$. The value $u(t, x)$ represents the deformation field and $T(t, x)$ the workpiece temperature.

We consider a milling process proceeding in the time interval $[0, t_e]$. The cutter has N_z teeth and rotates $N_r = n/t_e$ rounds in the respective time interval. With the rotation speed n, we define the rotation angle of tooth 'j' by $\varphi^j(t) = 2\pi nt + 2(j-1)\pi/N_z$, where $j = 1, 2, \ldots, N_z$. Note that the cutter considered here has straight edges. For a helix cutter an additional term has to be added to the latter equation.

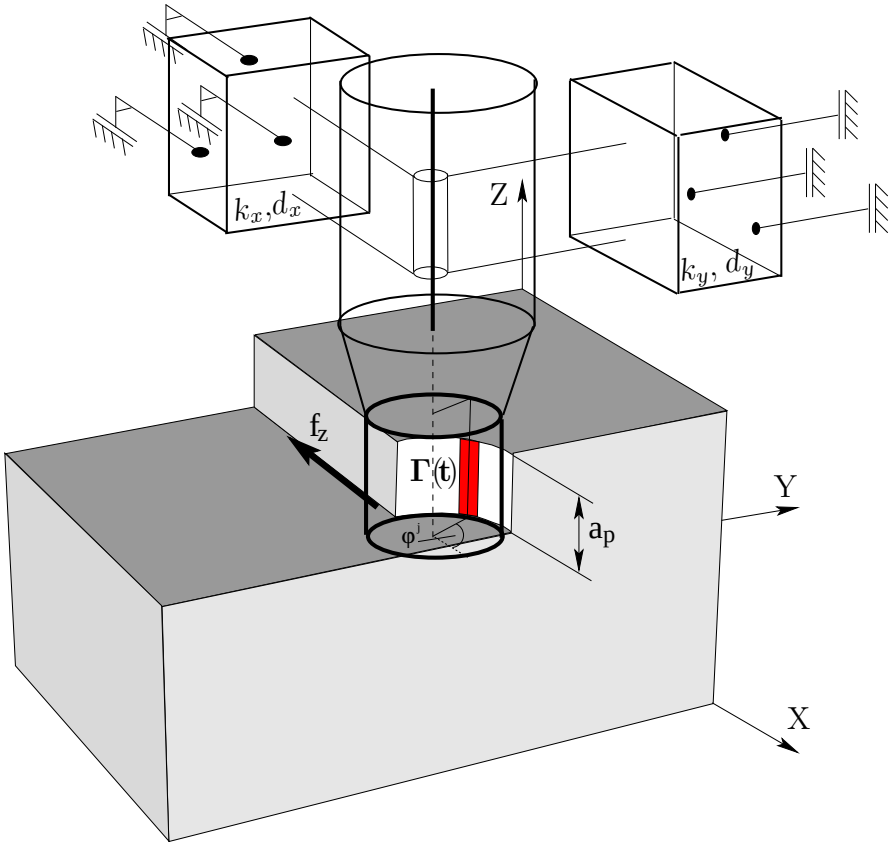

Figure 1: Schematic representation of the milling process.

Moreover, we initialize the rotation angle of the first tooth as $\varphi^1(0) = \varphi_S$, where φ_S is the entry angle at which the cutter first touches the workpiece. The tooth period $\tau = (nN_z)^{-1}$ is defined as the time the cutter needs to rotate around the pitch angle $2\pi/N_z$, i.e., the angle between two teeth. Another characteristic value in milling is the feed per tooth f_z, the distance that the cutter covers during one tooth period. The cutter removes material from the workpiece if the angle $(\varphi^j(t) \bmod 2\pi)$ is greater then the entry angle φ_S and smaller than the exit angle φ_E.

During the milling process, the cutting forces arising from the chip removal act on the cutter and on the workpiece simultaneously. Furthermore, the generated heat flows partly into the workpiece. These effects occur in vicinity of the cutting edge. Thus, the zone $\Gamma(t)$, where the cutting stress acts on and the heat flows into the work piece is not constant but moves with the cutting edge (cf. Figure 1).

2.2 Model equations

2.2.1 Milling machine

The milling cutter has a mass m_c and the coordinates $q = (q_x, q_y, q_z)^T$ measure the movement of its centre of mass with respect to the inertial reference frame (x, y, z). Note that the cutter oscillates in the x, y-plane. The additional z-component has been introduced to ease the coupling with the workpiece model to be discussed later. The coordinates in the cutter reference frame are related to those of the workpiece reference frame by a linear, time dependent transformation,

$$(x, y, z) = (X, Y, Z) - b(t), \tag{2.1}$$

where $b(t) = (X_0 - f_z \frac{t}{\tau}, Y_0, Z_0)$ denotes the translation vector given in the workpiece frame. With these preliminaries we get, according to Newton's second law, the equation of motion for the cutter model:

$$\ddot{q} + \begin{bmatrix} 2\xi_1\omega_1 & 0 & 0 \\ 0 & 2\xi_2\omega_2 & 0 \\ 0 & 0 & 0 \end{bmatrix} \dot{q} + \begin{bmatrix} \omega_1^2 & 0 & 0 \\ 0 & \omega_2^2 & 0 \\ 0 & 0 & 1 \end{bmatrix} q = \frac{1}{m_c} \begin{bmatrix} F_x \\ F_y \\ 0 \end{bmatrix}, \tag{2.2}$$

where the Eigen angular frequencies in x- and y-direction are denoted by $\omega_i = 2\pi f_i = \sqrt{\frac{k_i}{m_c}} > 0$. The modal damping in each direction is represented by $\xi_i = \frac{d_i}{2m_c k_i} > 0$. The right hand side of (2.2) takes into account the cutting force, a sum of the forces acting on each tooth in cut.

2.2.2 Workpiece

We assume that the largest part of the workpiece behaves like a thermoelastic material. Only in the vicinity of the cutting edge, visco-elasto-plastic effects have to be taken into account. However, these effects are already included in the empirical cutting force model, which means that we may focus here on the thermo-elastic behaviour of the workpiece.

The corresponding equations read as follows (see, e.g., [7]):

$$u_{tt} = \frac{1}{\varrho}\mathrm{div}(\sigma), \tag{2.3}$$

$$\sigma = \lambda tr(\varepsilon)I + 2\mu\varepsilon - 3K\alpha(T - T_0)I \quad \text{with} \quad K = (\lambda + \frac{2}{3}\mu), \tag{2.4}$$

$$\varepsilon = \frac{1}{2}\left(\nabla u + (\nabla u)^T\right), \tag{2.5}$$

$$\varrho c_v T_t = \kappa\Delta T - 3K\alpha T_0 \mathrm{div}(u_t), \tag{2.6}$$

where λ and μ are the Lamé constants, T_0 denotes the initial temperature, κ the heat conductivity and α is the thermal expansion coefficient.

2.3 Coupling

2.3.1 Boundary Conditions

The basis for the coupling of workpiece and machine model is the cutting force. Usually, the latter is computed in terms of the so-called *uncut chip thickness* (see, e.g., [1]), which describes the thickness of the material to be removed by the tooth which is in cut (see Sec. 2.3.2). Here we use the following algebraic relation between uncut chip thickness and the cutting forces due to Weck [13]):

$$\hat{F} = \left(\hat{F}_R, \hat{F}_T, \hat{F}_Z\right)^T = a_P \hat{K}(\bar{T}, v_{CS}) \max(h, 0), \tag{2.7}$$

where $\hat{K}(\bar{T}, v_{CS})$ denotes the vector of cutting constants which can be a function of cutting speed (cf. Faassen [5]) and of the temperature in the cutting zone. Note that the precise form of $\hat{K}(\bar{T}, v_{CS})$ has to be found experimentally. On the cutting edge the forces act in three directions: perpendicular to the cutting velocity, in opposite direction to the cutting velocity and parallel to the rotation axis of the cutter. Note that the z-component of $\hat{K}(\bar{T}, v_{CS})$ vanishes for orthogonal cutting. We transform equation (2.7) into the workpiece reference frame and sum up for all teeth to obtain

$$F = (F_x, F_y, F_z)^T = -\sum_{j=1}^{N_z} g(\varphi^j(t)) O(\varphi^j(t)) \hat{F}, \tag{2.8}$$

$$\text{with} \quad O(\varphi^j) = \begin{bmatrix} \cos\varphi^j & -\sin\varphi^j & 0 \\ \sin\varphi^j & \cos\varphi^j & 0 \\ 0 & 0 & 1 \end{bmatrix}.$$

Here, $g = 1$, if the corresponding tooth 'j' is in cut and $g = 0$ otherwise. The orthogonal matrix $O(\varphi^j)$ transforms the forces $\hat{F}$ into the workpiece reference frame.

Now we define the boundary condition for the momentum balance (cf. (2.6)) as:

$$\begin{aligned} u &= 0 \qquad \text{on} \qquad \Gamma_D, \\ \sigma \cdot n &= \begin{cases} \frac{F}{|\Gamma(t)|} & \text{on } \Gamma(t) \times (0, t_e). \\ 0 & \text{otherwise.} \end{cases} \end{aligned} \tag{2.9}$$

$|\Gamma(t)|$ denotes the measure of the area, where the cutting force acts on the workpiece (cf. Figure 1).

The boundary condition for the energy balance has a similar structure:

$$\begin{aligned} T &= T_0 \qquad \text{on} \qquad \Gamma_D, \\ -\kappa \nabla T \cdot n &= \begin{cases} Q_{HF}\left(t, \hat{F}, v_{CS}\right) & \text{on } \Gamma(t) \times (0, t_e), \\ 0 & \text{otherwise.} \end{cases} \end{aligned} \tag{2.10}$$

The value $v_{CS} = \pi D n$ denotes the cutting speed, i.e. the tangential velocity at the cutting edge. Finally, we have to estimate the heat flux into the workpiece, Q_{HF}. During material removal, the chip experiences large plastic deformations and high deformation rates. Since the elastic deformations are negligible we assume that the cutting energy is completely transformed into heat, which flows into the cutter, the chip and the workpiece. Thus we need to estimate the portion of the cutting heat that flows into the work piece. We assumed orthogonal cutting, which means that the cutting forces do not depend on the z-direction. Hence, on each x,y-level we have the same cutting conditions as in turning, such that we can apply the results of [11] leading to the following expression for the heat flux:

$$Q_{HF} = -\big(2\beta_{Fr2} + \beta_{Sh2}\big)\frac{c_T l_{c2} v_{CS} \hat{F}_T}{3h} + \beta_{Ch}(F_s v_s + F_u v_C), \tag{2.11}$$

where we used the abbreviations

$$F_s = \hat{F}_T^* \cos(\Phi_C) - \hat{F}_R^* \sin(\Phi_C), \tag{2.12}$$

$$F_u = \hat{F}_T^* \cos(\alpha_R) - \hat{F}_R^* \sin(\alpha_R), \tag{2.13}$$

$$\hat{F}_R^* = \big(1 - \frac{c_R l_{c2}}{h}\big)\hat{F}_R, \tag{2.14}$$

$$\hat{F}_T^* = \big(1 - \frac{c_T l_{c2}}{h}\big)\hat{F}_T. \tag{2.15}$$

The velocities are related to the cutting speed v_{CS} as follows:

$$v_s = v_{CS}\frac{\cos(\alpha_R)}{\cos(\Phi_C - \alpha_R)}, \tag{2.16}$$

$$v_C = v_{CS}\frac{\sin(\Phi_C)}{\cos(\Phi_C - \alpha_R)}, \tag{2.17}$$

with the approximate shear angle derived by Ernst and Merchant [4], $\Phi_C = \pi/4 - \delta_\Phi/2$ or by Lee and Schafer [10]: $\Phi_C = \pi/4 - \delta_\Phi$, and δ_Φ given by

$$\delta_\Phi = \arctan\left(\frac{\hat{F}_R^*}{\hat{F}_T^*}\right). \tag{2.18}$$

Note that, according to Altintas [1], α_R denotes the rake angle of the cutting edge, a value that describes the cutter geometry. The remaining parameters l_{c2}, c_T, c_R, β_{Fr2}, β_{Sh2} and β_{Ch} are either given by Harris [6] or they have to be determined experimentally.

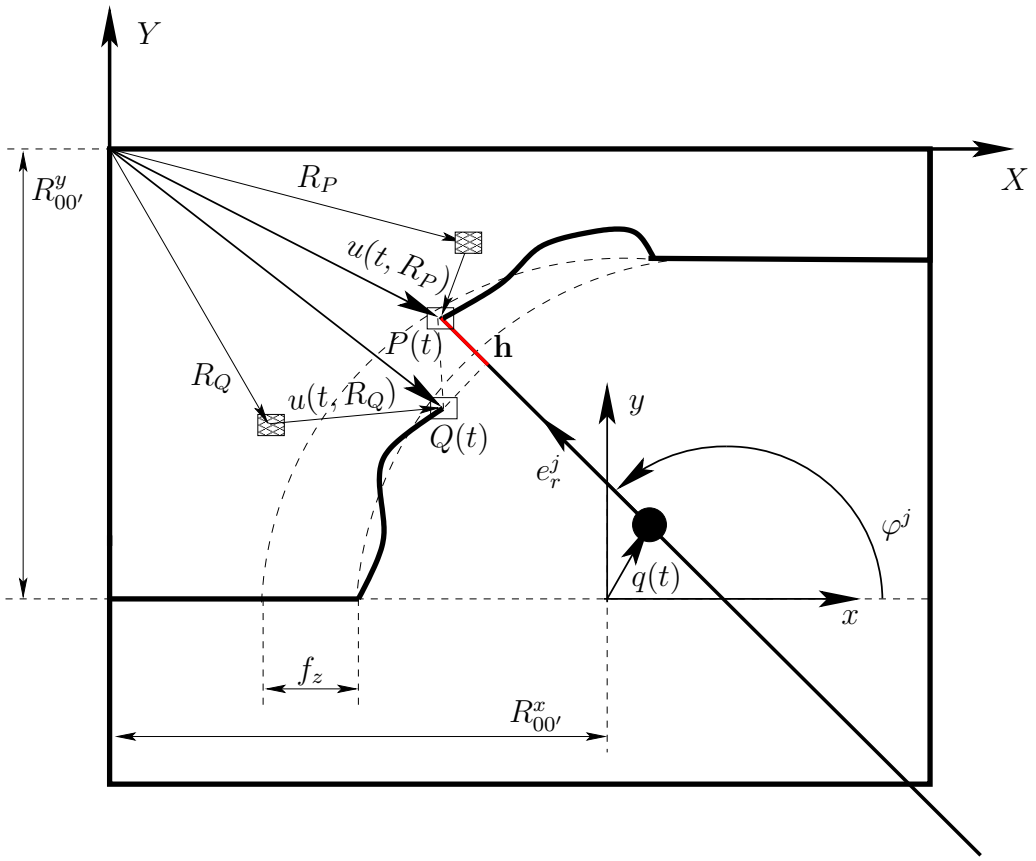

Figure 2: Derivation of the uncut chip thickness.

2.3.2 Uncut chip thickness

The crucial point is to derive an expression for the uncut chip thickness h. To this end, we look at a $z = const$ plane and assume that cutter and work piece may oscillate independently (cf. Figure 2). At time t the cutter marks with its tip a certain material point R_P of the workpiece moved to its position due to the deformation field $u(t, R_P)$. Thus, we may express the point $P(t)$ using on the one hand the workpiece kinematics and on the other hand the cutter position:

$$\begin{aligned} P(t) &= u(t, R_P) + R_P, \\ &= R_{00'}(t) + \frac{D}{2} e^j_r + q(t), \end{aligned} \tag{2.19}$$

where D denotes the diameter of the cutter. Usually, the uncut chip thickness is defined as:

$$h = (P(t) - Q(t)) \cdot e^j_r, \tag{2.20}$$

with $e^j_r = (\cos\varphi^j, \sin\varphi^j, 0)^T$ representing the unit vector in radial direction of tooth 'j' at time t. $Q(t)$ represents the relevant part of the workpiece surface created during the

preceding cut. Recall that at time $t-\tau$ the cutter marked another material point R_Q that was moved to its position due to the deformation field $u(t-\tau, R_Q)$. Thus equation (2.19) also holds at time $t-\tau$, i.e.,

$$u(t-\tau, R_Q) + R_Q = R_{00'}(t-\tau) + \frac{D}{2}e_r^j + q(t-\tau). \tag{2.21}$$

Furthermore, it is clear that the material point R_Q is also subjected to the workpiece deformation field $u(t, R_Q)$ at time t , which means that it is located at position

$$Q(t) = u(t, R_Q) + R_Q.$$

For better visibility, the distance between the material points R_P and R_Q has been artificially magnified in Figure 2. In fact, they are quite close. In particular, it is fair to assume that the difference in displacement fields for Q and P is small, i.e.

$$u(t, R_Q) \approx u(t, R_P),$$

then we obtain

$$Q(t) = u(t, R_P) + R_Q. \tag{2.22}$$

Finally, we replace R_Q in equation (2.22) using equation (2.21), which yields the expression

$$Q(t) = q(t-\tau) + u(t, R_P) - u(t-\tau, R_Q) + R_{00'}(t-\tau) + \frac{D}{2}e_r^j. \tag{2.23}$$

Using (2.19), we obtain

$$P(t) - Q(t) = R_{00'}(t) - R_{00'}(t-\tau) + q(t) - q(t-\tau) - u(t, R_P) - u(t-\tau, R_Q). \tag{2.24}$$

leading to the following expression for the uncut chip thickness:

$$h = -f_z \cos\varphi^j + (q(t) - q(t-\tau)) \cdot e_r^j - (u(t, R_P) - u(t-\tau, R_Q)) \cdot e_r^j. \tag{2.25}$$

We notice that the uncut chip thickness consists of three different parts. The first one represents just the cutter displacement due to the given feed. Projected on the radial direction, it yields the stationary uncut chip thickness. The second part represents the machine oscillations and produces the modulation of the chip thickness that has been identified to be the main reason for chatter. The third contribution to the uncut chip thickness is related to the workpiece deformation. While the first two terms are well-known, the third one is new. With this approach, for the first time, the influence of complex workpiece dynamics on the stability of milling processes can be studied.

3 Analysis of the coupled system

In this section we assume that the feeding velocity f_z of the cutter is equal to zero. Then the dominating term in the uncut chip thickness (2.25) vanishes and it is fair to assume that the workpiece geometry remains unchanged during the process. In this situation the cutter tip acts on the workpiece as a time dependent force boundary condition.

To analyse the coupled PDE/DDE system we use the method of steps. To this end, we divide the time interval $[0, t_e]$ into subintervals with the length τ, tacitly assuming t_E to be a multiple of τ. For given initial data on the interval $[-\tau, 0]$ we analyse the system in $[0, \tau]$. Then iteratively, we use the solution in $[(l-1)\tau, l\tau]$ as initial data for the following tooth period and perform the analysis for the interval $[l\tau, (l+1)\tau]$.

We assume $\Omega \subset \mathbb{R}^3$ to be a bounded domain with Lipschitz boundary, and $\partial\Omega = \Gamma_0 \cup \Gamma(t) \cup \Gamma_R(t)$ where $meas(\Gamma_0) > 0$ and the part Γ_0 is constant in time. $\Gamma(t)$ is a part of the boundary whose evolution in time is known and there exist constants Γ_1, $\Gamma_2 > 0$ such that $\Gamma_1 < meas(\Gamma(t)) < \Gamma_2$ for all times. Moreover, $\Gamma_R(t) = \partial\Omega \backslash (\Gamma_0 \cup \Gamma(t))$ and $meas(\Gamma_R(t)) > 0$ for all times. In the space-time cylinder $\Omega \times (l\tau, (l+1)\tau)$ we consider the following system of equations from linear thermoelasticity in the dynamical setting:

$$\begin{aligned} \varrho\ddot{u}(x,t) - \operatorname{div}\sigma(x,t) &= 0 && (3.1)\\ \sigma(x,t) &= A(\varepsilon(u(x,t)) - \varepsilon^{th}(x,t)) + \delta\varepsilon(\dot{u}(x,t)) && (3.2)\\ \varrho c_v \dot{T}(x,t) - \operatorname{div}(\kappa\nabla T(x,t)) &= -3K\alpha T_0(x)\operatorname{div}\dot{u}(x,t), && (3.3) \end{aligned}$$

where ϱ, c_v, K, α have already been introduced in Section 2.2.2 and δ is a constant, $A_{ijkl} = \lambda\delta_{ij}\delta_{kl} + \mu(\delta_{il}\delta_{jk} + \delta_{jl}\delta_{ik})$ is the constant elasticity tensor, and T_0 is the initial temperature. The system is studied with the following initial conditions for $l > 0$:

$$u(x, l\tau) = u^{l-1}(x, l\tau), \quad \dot{u}(x, l\tau) = \dot{u}^{l-1}(x, l\tau), \quad T(x, l\tau) = T^{l-1}(x, l\tau), \tag{3.4}$$

where (u^{l-1}, T^{l-1}) is the solution on $\Omega \times ((l-1)\tau, l\tau)$. If $l = 0$ we use the initial conditions

$$u(x,0) = u_0, \quad \dot{u}(x,0) = u_1, \quad T(x,0) = T_0(x), \tag{3.5}$$

for which we assume

$$u_0 \in V, \quad u_1 \in L^2(\Omega;\mathbb{R}^3), \quad T_0 \in L^\infty(\Omega),$$

with $V = \{v \in H^1(\Omega;\mathbb{R}^3) : v_{\big|\Gamma_0} = 0\}$.

As detailed in the previous section the coupling between cutter and workpiece dynamics is realized through the cutting force (cf. (2.7), (2.8)), which enters the boundary conditions for the momentum balance (2.9) as well as the one for the energy balance (2.10). The crucial part here is the uncut chip thickness h which is defined in (2.25). Since we assume that the cutting forces act on the surface part $\Gamma(t)$, we replace h in the cutting force model (2.7) by its mean value on $\Gamma(t)$. To this end, we define the mean values $\bar{u}$, $\bar{T}$ by

$$\bar{u}(t) = \fint_{\Gamma(t)} u(x,t)dS(x), \quad \bar{T}(t) = \fint_{\Gamma(t)} T(x,t)dS(x).$$

This allows to rewrite the boundary condition for the momentum balance as

$$\begin{aligned} u(x,t)_{\big|\Gamma_0} &= 0\\ \sigma(x,t)\nu(x) &= \begin{cases} 0 & \text{on } \Gamma_R(t)\\ f_2(q(t), q(t-\tau), \bar{u}(t), \bar{u}(t-\tau), \bar{T}(t)) & \text{on } \Gamma(t) \end{cases} \end{aligned} \tag{3.6}$$

We assume that the given function f_2 is a global Lipschitz function. Moreover, $\bar{u}(t-\tau)$ is defined by

$$\bar{u}(s) \;=\; \bar{u}^{l-1}(s) \quad \text{for } s \in [(l-1)\tau, l\tau], \tag{3.7}$$

where u^{l-1} corresponds to the solution on $[(l-1)\tau, l\tau]$. For $l=0$ we define

$$\bar{u}(s) \;=\; \omega_2(s) \quad \text{for } s \in [-\tau, 0], \tag{3.8}$$

where ω_2 is a given smooth function.

Similarly, the boundary conditions for the energy balance are rewritten as

$$\kappa \frac{\partial T}{\partial \nu}(x,t) = \begin{cases} -\alpha_H(T(x,t) - T_T) & \text{on } \Gamma_0 \\ f_1(q(t), q(t-\tau), \bar{u}(t), \bar{u}(t-\tau), \bar{T}(t)) & \text{on } \Gamma(t) \\ 0 & \text{on } \Gamma_R(t) \end{cases} \tag{3.9}$$

where κ, T_T are positive constants and the given function f_1 is globally Lipschitz. Finally, $q : (l\tau, (l+1)\tau) \longrightarrow \mathbb{R}^3$ is the solution to the DDE, describing the movement of the centre of mass of the milling cutter, cf. (2.2), which we rewrite as

$$\ddot{q}(t) + D\dot{q}(t) + Kq(t) = B(t, \bar{T}(t))(q(t) - q(t-\tau) - \bar{u}(t) + \bar{u}(t-\tau)) \tag{3.10}$$

with the following initial condition for $l > 0$:

$$q(s) \;=\; q^{l-1}(s) \quad \text{for } s \in [(l-1)\tau, l\tau] \tag{3.11}$$

where (u^{l-1}, q^{l-1}) correspond to the solution on $[(l-1)\tau, l\tau]$. For $l=0$ we define

$$q(s) \;=\; \omega_1(s) \quad \text{for } s \in [-\tau, 0] \tag{3.12}$$

where ω_1 is a given smooth function with vanishing z-component.

In view of Section 2.2.1 the matrices D, K are symmetric and positive definite and the matrix B is globally Lipschitz. In the sequel, we will drop the explicit time dependency in the arguments of f_1, f_2, respectively. The retarded argument is indexed by τ, e.g., $q_\tau := q(t-\tau)$.

Remark 3.1 *(1) On the space-time domain $\Omega \times (l\tau, (l+1)\tau)$ our initial boundary-value problem is a coupling of linear thermoelasticity with a linear ODE for the vector q. The entire problem is nonlinear because of Lipschitzian nonlinearities in the Neumann boundary condition on $\Gamma(t)$ and of the quadratic right-hand side in the system for the vector q.*

(2) In comparison to the system derived in Section 2, we had to add a regularising damping term in the momentum balance, assumed to be small.

(3) To simplify the notations, without loss of generality it is sufficient to study the problem only for the first step. Hence, in the sequel we consider the problem on $\Omega \times (0, \tau)$.

The goal of this section is to prove global in time solvability of the considered initial boundary-value problem. We start with a weak formulation. The first equation in the weak form is given by the equality

$$\begin{aligned}\langle \varrho \ddot{u}(t), v\rangle + \int_\Omega A\varepsilon(u(t))\varepsilon(v)dx + \delta\int_\Omega \varepsilon(\dot{u}(t))\varepsilon(v)dx \\ = \int_\Omega A\varepsilon^{th}(t)\varepsilon(v)dx + \int_{\Gamma(t)} f_2(q, q_\tau, \bar{u}, \bar{u}_\tau, \bar{T})vdS\end{aligned} \tag{3.13}$$

for all $v \in V$ and for almost $t \in (0, \tau)$. We suppose that the thermal part of the strain tensor has the diagonal form

$$\varepsilon^{th} = \alpha(T - T_0)I =: \beta(T)I,$$

where $\alpha > 0$ is the thermal expansion coefficient. Since $AI = 3KI$, the first integral on the right-hand side of (3.13) has the form

$$3K\int_\Omega \beta(T(t))\,\mathrm{div}\, v dx.$$

In (3.13) the symbol $\langle\cdot,\cdot\rangle$ denotes the duality form between the spaces V^* and V. The second equation written in the weak sense has the form

$$\begin{aligned}\langle \varrho c_v\dot{T}(t), w\rangle + \int_\Omega \kappa\nabla T(t)\nabla w dx = -3K\alpha\int_\Omega T_0\,\mathrm{div}\,\dot{u}(t)w dx \\ - \int_{\Gamma_0}\alpha_H(T(t) - T_T)w dS + \int_{\Gamma(t)} f_1(q, q_\tau, \bar{u}, \bar{u}_\tau, \bar{T})w dS\end{aligned} \tag{3.14}$$

for all $w \in H^1(\Omega)$ and for almost all $t \in (0, \tau)$. Here the symbol $\langle\cdot,\cdot\rangle$ denotes the duality form between the spaces $(H^1(\Omega))^*$ and $H^1(\Omega)$. Hence we consider two variational equalities (3.13) and (3.14) coupled with the system of ordinary differential equations (3.10) with initial conditions (3.5) and (3.11). To prove existence of weak solutions to the considered problem we use the Galerkin method. Let us denote by $\{v_1, v_2, \ldots\}$ a basis of V such that the functions v_i are orthogonal in $H^1(\Omega)$ and orthonormal in $L^2(\Omega)$. Next let us denote by $\{w_1, w_2, \ldots\}$ a basis of $H^1(\Omega)$ such that w_i are orthogonal in $H^1(\Omega)$ and orthonormal in $L^2(\Omega)$. We want to construct a Galerkin approximation of a weak solution and denote by

$$u^n(x,t) = \sum_{k=1}^n d_n^k(t)v_k(x)\,,\ T^n(x,t) = \sum_{k=1}^n \gamma_n^k(t)w_k(x)\,.$$

We require that functions u^n and T^n satisfy (3.13) and (3.14) on the spaces $V_n = \mathrm{lin}\,\{v_1, \ldots v_n\}$, $W_n = \mathrm{lin}\,\{w_1, \ldots w_n\}$ respectively. Recall that q_τ and $\bar{u}_\tau$ are already given either as initial conditions or by the previous step. This implies that we obtain the following system of ordinary differential equations for the unknown coefficients d_n^k, γ_n^k for $k = 1, 2, \ldots n$

$$\begin{aligned}\varrho\ddot{d}_n^k(t) + \sum_{i=1}^n d_n^i(t)\int_\Omega A\varepsilon(v_i)\varepsilon(v_k)dx + \delta\sum_{i=1}^n \dot{d}_n^i(t)\int_\Omega \varepsilon(v_i)\varepsilon(v_k)dx \\ = 3K\int_\Omega \beta(T^n)\,\mathrm{div}\, v_k dx + \int_{\Gamma(t)} f_2(q^n, q_\tau, \bar{u}^n, \bar{u}_\tau, \bar{T}^n)v_k dS\end{aligned} \tag{3.15a}$$

$$\varrho c_v \dot{\gamma}_n^k(t) + \kappa \gamma_n^k(t) \|\nabla w_k\|^2_{L^2(\Omega)} = -3K\alpha \sum_{i=1}^{n} \dot{d}_n^i(t) \int_\Omega T_0 \operatorname{div} v_i w_k dx$$
$$- \int_{\Gamma_0} \alpha_H (T^n(t) - T_T) w_k dS + \int_{\Gamma(t)} f_1(q^n, q_\tau, \bar{u}^n, \bar{u}_\tau, \bar{T}^n) w_k dS \tag{3.15b}$$

where q^n is a solution of the system

$$\ddot{q}^n(t) + D\dot{q}^n(t) + Kq(t) = B(t, \bar{T}^n(t))(q^n - q_\tau - \bar{u}^n + \bar{u}_\tau) \tag{3.15c}$$

with the initial conditions

$$d_n^k(0) = (u_0, v_k), \quad \dot{d}_n^k(0) = (u_1, v_k), \quad \gamma_n^k(0) = (T_0, w_k)\,, \ k = 1, 2, \dots n$$

and for $q^n(s), \bar{u}^n(s)$ in $[-\tau, 0]$ according to (3.12), (3.8). Assuming that the given function $t \mapsto \Gamma(t)$ is continuous with respect to the Hausdorff metric we see that the considered system of $2n+3$ ordinary differential equations possesses a unique solution defined on the time interval $(0, t_n)$. Moreover, we can assume, if $w_1(s) \in B_{M/2}(0)$ for each $s \in [-\tau, 0]$ then $q^n(t) \in B_M(0)$ for all $t \in (0, t_n)$. Here, $B_r(z)$ denotes the open Ball in $\mathbb{R}^3$ with radius r and centre z.

Next, we find some conditions such that the sequence $\{t_n\}$ will be bounded from below by some positive constant.

Lemma 3.1 *Assume that $w_1, w_2 \in B_{M/2}(0)$ and that there exists a positive constant $C(M, t^*)$ such that $|\bar{u}^n| + \int_0^{t_n} |T^n|^2 dt \le C(M, t^*)$ for all $t_n \le t^*$ and all n. Then there exists $\tau_+ > 0$ such that $t_n \ge \tau_+$ for all n.*

Proof: Testing (3.15c) by $\dot{q}^n$ we have

$$\frac{d}{dt}\frac{1}{2}|\dot{q}^n|^2 + D\dot{q}^n \cdot \dot{q}^n + Kq^n \cdot \dot{q}^n = B(t, \bar{T}^n)(q^n - q_\tau - \bar{u}^n + \bar{u}_\tau) \cdot \dot{q}^n. \tag{3.16}$$

Using that B is global Lipschitz we conclude that $|B(t, \bar{T}^n)| \le C(1 + |t| + |\bar{T}^n|)$. Using this inequality we can estimate the right-hand side of (3.16) by

$$\begin{aligned} C(1 + |t| + |\bar{T}^n|)(2M + |\bar{u}^n|)|\dot{q}^n| \le 6M^2C^2(1 + |t|^2 + |\bar{T}^n|^2) + \frac{1}{2}|\dot{q}^n|^2 \\ + \frac{3}{2}C^2(1 + |t|^2 + |\bar{T}^n|^2)|\bar{u}^n|^2 + \frac{1}{2}|\dot{q}^n|^2\,. \end{aligned} \tag{3.17}$$

Inserting (3.17) into (3.16) integrating in time over $(0, t_n)$ and using Gronwall inequality we have

$$\begin{aligned} \frac{1}{2}|\dot{q}^n(t^n)|^2 + \int_0^{t_n} D\dot{q}^n \cdot \dot{q}^n dt + \frac{1}{2}Kq^n(t^n) \cdot q^n(t^n) \le e^{2t_n}\bigg(\frac{1}{2}|\dot{q}^n(0)|^2 + \frac{1}{2}Kq(0) \cdot q(0) \\ + \int_0^{t_n} 6M^2C^2(1 + |t|^2 + |\bar{T}^n|^2)dt + \int_0^{t_n} \frac{3}{2}C^2(1 + |t|^2 + |\bar{T}^n|^2)|\bar{u}^n|^2 dt\bigg)\,. \end{aligned} \tag{3.18}$$

K is symmetric and positive definite hence there exists a positive constant K^* such that $K^*|q|^2 \le Kq \cdot q$ for all $q \in \mathbb{R}^3$. By the assumption we have that $|\bar{u}^n|$ is bounded on finite

time intervals and also $\int_0^{t_n} |T^n|^2 dt$ is bounded if $t_n \leq t^*$. Then the right-hand side for $t_n \leq t^*$ is bounded. This means that $q^n(t)$ and $\dot{q}^n(t)$ for $t_n \leq t^*$ stay in a bounded set $B_{\bar{C}(M,t^*)}(0)$. Moreover, we see that in the nonlinear terms f_1, f_2 in the system (3.15) the arguments q^n, q^n_τ are bounded for $t_n \leq t^*$. Then the solution of the system (3.15) exists at least on the interval $[0, t^*]$. t^* can be chosen arbitrary and the proof is complete. ∎

Now we are going to prove that the assumption from the last lemma holds. To this end we multiply (3.15a) by $\dot{d}^k_n$, (3.15b) by γ^k_n and sum the results with respect to k. Hence we obtain the following two equalities

$$\begin{aligned} &\varrho \frac{d}{dt} \frac{1}{2} \|\dot{u}^n(t)\|^2_{L^2(\Omega)} + \int_\Omega A\varepsilon(u^n(t))\varepsilon(\dot{u}^n(t))dx + \delta \int_\Omega |\varepsilon(\dot{u}^n(t))|^2 dx \qquad (3.19a) \\ &= 3K \int_\Omega \beta(T^n(t)) \operatorname{div} \dot{u}^n(t) dx + \int_{\Gamma(t)} f_2(q^n, q_\tau, \bar{u}^n, \bar{u}_\tau, \bar{T}^n) \dot{u}^n(t) dS\,, \\ &\varrho c_v \frac{d}{dt} \|T^n(t)\|^2_{L^2(\Omega)} + \kappa \int_\Omega |\nabla T^n(t)|^2 dx = -3K\alpha \int_\Omega T_0 \operatorname{div} \dot{u}^n(t) T^n(t) dx \qquad (3.19b) \\ &- \int_{\Gamma_0} \alpha_H (T^n(t) - T_T) T^n(t) dS + \int_{\Gamma(t)} f_1(q^n, q_\tau, \bar{u}^n, \bar{u}_\tau, \bar{T}^n) T^n(t) dS\,. \end{aligned}$$

Since the functions f_i are globally Lipschitz, we can conclude that there exist positive constants $C_i > 0$ such that

$$|f_i(q, q_\tau, \bar{u}, \bar{u}_\tau, \bar{T})| \leq C_i(1 + |q| + |q_\tau| + |\bar{u}| + |\bar{u}_\tau| + |\bar{T}|)$$

for all arguments q, q_τ, $\bar{u}$, $\bar{u}_\tau$, $\bar{T}$. Next, we estimate integrals on the right-hand side of (3.19a):

$$3K \int_\Omega \beta(T^n(t)) \operatorname{div} \dot{u}^n(t) dx \leq \frac{\delta}{8} \| \operatorname{div} \dot{u}^n(t)\|^2_{L^2(\Omega)} + C(\delta)(1 + \|T^n(t)\|^2_{L^2(\Omega)}) \qquad (3.20)$$

$$\begin{aligned} &\int_{\Gamma(t)} f_2(q^n, q_\tau, \bar{u}^n, \bar{u}_\tau, \bar{T}^n) \dot{u}^n(t) dS \\ &\quad \leq (1 + 2M + |\bar{T}^n(t)| + |\bar{u}^n(t)|) \int_{\Gamma(t)} |\dot{u}^n(t)| dS \end{aligned} \qquad (3.21)$$

(we have used here that from definition of t_n we have $|q^n(t)|$ and $|q_\tau|$ are bounded by M for $t \leq t_n$). Since the measure of $\Gamma(t)$ is positive and bounded we have

$$\int_{\Gamma(t)} |\dot{u}^n(t)| dS \leq |\Gamma(t)|^{1/2} \|\dot{u}^n(t)\|_{L^2(\Gamma(t))}\,, \qquad (3.22)$$

$$|\bar{T}^n(t)| = \left| \fint_{\Gamma(t)} T^n(t) dS \right| \leq \frac{1}{|\Gamma(t)|} \int_{\Gamma(t)} |T^n(t)| dS \leq \frac{1}{|\Gamma(t)|^{1/2}} \|T^n(t)\|_{L^2(\Gamma(t))}\,. \qquad (3.23)$$

Inserting (3.22), (3.23) into (3.21) and estimating $|\bar{u}^n(t)|$ in the same manner as $|\bar{T}^n(t)|$

we can invoke the trace theorem to arrive at the inequality

$$\begin{aligned}
&\int_{\Gamma(t)} f_2(q^n, q_\tau^n, \bar{u}^n, \bar{u}_\tau^n, \bar{T}^n)\dot{u}^n(t)dS \le \Gamma_2^{1/2}(1+2M)\|\dot{u}(t)\|_{L^2(\Gamma(t))} \\
&+ \Big(\|T^n(t)\|_{L^2(\Gamma(t))} + \|u^n(t)\|_{L^2(\Gamma(t))}\Big)\|\dot{u}^n(t)\|_{L^2(\Gamma(t))} \\
&\le C(\delta)\Gamma_2(1+2M)^2 + \frac{\delta}{8}\|\varepsilon(\dot{u}^n(t))\|^2_{L^2(\Omega)} \\
&+ C(\delta)\Big(\|T^n(t)\|^2_{L^2(\Gamma(t))} + \|\varepsilon(u^n(t))\|^2_{L^2(\Omega)}\Big) + \frac{\delta}{8}\|\varepsilon(\dot{u}^n(t))\|^2_{L^2(\Omega)}\,.
\end{aligned}$$

Finally, we estimate the boundary norm $\|T^n(t)\|^2_{L^2(\Gamma(t))}$ by

$$\|T^n(t)\|^2_{L^2(\Gamma(t))} \le \eta\|\nabla T^n(t)\|^2_{L^2(\Omega)} + C(\eta)\|T^n(t)\|^2_{L^2(\Omega)} \tag{3.24}$$

where $\eta > 0$ is arbitrary. Inequality (3.24) follows by the Ehrling lemma for the spaces $H^1(\Omega) \hookrightarrow H^{3/4}(\Omega) \hookrightarrow L^2(\Omega)$. (Note that the trace operator is continuous from $H^{3/4}(\Omega)$ into $L^2(\partial\Omega)$). To estimate the integrals on the right-hand side of (3.19b) we note that by the boundedness of T_0 the first term can be estimated in the same manner as in (3.20) and the last term as in (3.21). Invoking Young's inequality, the second term leads to

$$\begin{aligned}
-\int_{\Gamma_0} \alpha_H(T^n(t) - T_T)T^n(t)dS &= -\alpha_H\|T^n(t)\|^2_{L^2(\Gamma_0)} + \alpha_H\int_{\Gamma_0} T_T T^n(t)dS \\
&\le -\frac{\alpha_H}{2}\|T^n(t)\|^2_{L^2(\Gamma_0)} + \frac{\alpha_H}{2}|\Gamma_0|T_T^2\,.
\end{aligned} \tag{3.25}$$

Inserting all estimates into (3.19) and adding (3.19a) and (3.19b) we arrive at the inequality

$$\begin{aligned}
&\varrho\frac{d}{dt}\frac{1}{2}\|\dot{u}^n(t)\|^2_{L^2(\Omega)} + \frac{d}{dt}\frac{1}{2}\int_\Omega A\varepsilon(u^n(t))\varepsilon(u^n(t))dx + \delta\|\varepsilon(\dot{u}^n(t))\|^2_{L^2(\Omega)} \\
&\qquad + \varrho c_v\frac{d}{dt}\|T^n(t)\|^2 + \kappa\|\nabla T^n(t)\|^2_{L^2(\Omega)} + \frac{\alpha_H}{2}\int_{\Gamma_0}|T^n(t)|^2dS \\
&\qquad \le \frac{\delta}{2}\|\varepsilon(\dot{u}(t))\|^2_{L^2(\Omega)} + \eta C_1(M,\delta)\|\nabla T^n\|^2_{L^2(\Omega)} \\
&\qquad + C_2(M,\delta)\|\varepsilon(u^n(t))\|^2_{L^2(\Omega)} + C_3(M,\delta,\eta)\|T^n(t)\|^2_{L^2(\Omega)} + C_4(M,\delta)
\end{aligned} \tag{3.26}$$

where $C_i(M,\delta)$ are positive constants. Choosing η so small that $\eta C_1(M,\delta) \le \frac{\kappa}{2}$, integrating (3.26) with respect to t on $(0,t)$ and using the Gronwall inequality we have proved the following theorem:

Lemma 3.2 *There exists a positive constant $C(M,t^*,\delta)$ such that for all u and for all $t_n \le t^*$*

$$\begin{aligned}
&\|\dot{u}^n(t)\|^2_{L^2(\Omega)} + \|\varepsilon(u^n(t))\|^2_{L^2(\Omega)} + \delta\int_0^t\|\varepsilon(\dot{u}^n(t))\|^2_{L^2(\Omega)}dt \\
&+ \|T^n(t)\|^2_{L^2(\Omega)} + \int_0^t\|\nabla T^n(t)\|^2_{L^2(\Omega)}dt + \int_0^t\int_{\Gamma_0}|T^n(t)|^2dS \\
&\le C(M,t^*,\delta) + \|u_0\|^2_{H^1(\Omega)} + \|u_1\|^2_{L^2(\Omega)}
\end{aligned} \tag{3.27}$$

for $t \in (0,t_n)$.

Remark 3.2 *Note that by the trace theorem we have that*

$$\sup_{t\in[0,t_n]}\|u^n(t)\|_{L^2(\Gamma(t))}+\int_0^{t^n}\|T^n(t)\|^2_{L^2(\Gamma(t))}$$

is bounded by a constant depending on M, t^* and δ only. Consequently, the assumption in Lemma 3.1 is satisfied.

In view of this remark our approximate solutions are defined globally in time. To pass to the limit with $n\to\infty$ we need some further estimates for the sequences $\{\dot T^n\}$ and $\{\ddot u^n\}$.

Lemma 3.3 *The sequences $\{\dot T^n\}$, $\{\ddot u^n\}$ are bounded in the spaces $L^2(0,\tau;H^1(\Omega)^*)$ and $L^2(0,\tau;V^*)$, respectively, where $\tau>0$.*

Proof: Let $w\in H^1(\Omega)$ and $\|w\|_{H^1(\Omega)}\le 1$. Let us decompose w in the form $w=w^1+w^2$ where $w^1\in W_n$ and $w^2\perp W_n$. Using that $w^1\in W_n$ we can use w^1 as a test function and obtain from (3.15b) that

$$\begin{aligned}&(\dot T^n(t),w^1)+\kappa\int_\Omega\nabla T^n(t)\nabla w^1dx=-3K\alpha\int_\Omega T_0\,\mathrm{div}\,\dot u^n w^1dx\\&-\int_{\Gamma_0}\alpha_H(T^n(t)-T_T)w^1dS+\int_{\Gamma(t)}f_1(q^n,q^n_\tau,\bar u^n,\bar u_\tau,\bar T^n)w^1dS\,.\end{aligned}\tag{3.28}$$

Using that $\dot T^n(t)\in W_n$ and $w^2\perp W_n$ we obtain that

$$\begin{aligned}&|(\dot T^n(t),w)|=|(\dot T^n(t),w^1)|\le\kappa\|\nabla T^n(t)\|_{L^2(\Omega)}\|\nabla w^1\|_{L^2(\Omega)}\\&+3K\alpha\sup|T_0|\|\,\mathrm{div}\,\dot u^n\|_{L^2(\Omega)}\|w^1\|_{L^2(\Omega)}+\alpha_H\|T^n(t)\|_{L^2(\Gamma_0)}\|w^1\|_{L^2(\Gamma_0)}\\&+\alpha_HT_T\|w^1\|_{L^2(\Gamma_0)}+C\big(1+2M+\|u^n(t)\|_{L^2(\Gamma(t))}+\|T^n(t)\|_{L^2(\Gamma(t))}\big)\|w^1\|_{L^2(\Gamma(t))}\end{aligned}$$

where the constant C depends on Γ_1. Using the trace theorem we arrive at the inequality

$$|(\dot T^n(t),w)|\le C(M)\big(\|\nabla T^n(t)\|_{L^2(\Omega)}+\|\varepsilon(\dot u^n(t))\|_{L^2(\Omega)}+\|T^n(t)\|_{L^2(\Omega)}+1\big)\,.$$

Consequently, we conclude that

$$\|\dot T^n(t)\|^2_{(H^1(\Omega))^*}\le 4C^2(M)\big(\|\nabla T^n(t)\|^2_{L^2(\Omega)}+\|\varepsilon(\dot u^n(t))\|^2_{L^2(\Omega)}+\|T^n(t)\|^2_{L^2(\Omega)}+1\big)\,.$$

Integrating the last inequality with respect to time and using theorem 3.2 we end the proof for the sequence $\{\dot T^n\}$. The proof for the sequence $\{\ddot u^n\}$ is similar and will be omitted. ∎

Theorem 3.1 *For each $\tau>0$ there exists a weak solution (u,T,q) of the considered problem. Moreover, we have that*

$$u\in L^\infty(0,\tau;V),\quad \dot u\in L^\infty(0,\tau;L^2(\Omega,\mathbb{R}^3))\cap L^2(0,\tau;V),\quad \ddot u\in L^2(0,\tau;V^*),$$

$$T\in L^\infty(0,\tau;L^2(\Omega)),\quad \nabla T\in L^2(0,\tau;L^2(\Omega;\mathbb{R}^n)),\quad \dot T\in L^2(0,\tau;(H^1(\Omega))^*)$$

$$q,\dot q\in L^\infty(0,\tau),\quad \ddot q\in L^2(0,\tau).$$

Proof: According to Lemma 3.2 and 3.3 we can choose a subsequence of $\{(u^n, T^n, q^n)\}$, further denoted by index n, such that

$$\begin{aligned}
&u^n \overset{*}{\rightharpoonup} u \quad \text{in } L^\infty(0,\tau,V)\,, && \dot{u}^n \rightharpoonup \dot{u} \quad \text{in } L2\infty(0,\tau;V) \text{ and } L^\infty(0,\tau;L^2(\Omega,\mathbb{R}^3))\\
&\ddot{u}^n \rightharpoonup \ddot{u} \quad \text{in } L^2(0,\tau;V^*)\,, && T^n \overset{*}{\rightharpoonup} T \quad \text{in } L^\infty(0,\tau;L^2(\Omega))\\
&\nabla T^n \rightharpoonup \nabla T \quad \text{in } L^2(0,\tau;L^2(\Omega;\mathbb{R}^n))\,, && \dot{T}^n \rightharpoonup \dot{T} \quad \text{in } L^2(0,\tau;(H^1(\Omega))^*)\\
&q^n \to q \quad \text{in } L^\infty(0,\tau)\,, && \dot{q}^n \overset{*}{\rightharpoonup} \dot{q} \quad \text{in } L^\infty(0,\tau)\,,\ \ddot{q}^n \rightharpoonup \ddot{q} \quad \text{in } L^2(0,\tau)\,.
\end{aligned}$$

Note that boundedness of the sequence $\{\ddot{q}^n\}$ in $L^2(0,\tau)$ follows directly from equation (3.15c) and Theorem 3.2.

By virtue of the Aubin-Lions lemma (cf., e.g., [12]), we have that the sequence $\{T^n\}$ is precompact in the space $L^2(0,\tau;H^{3/4}(\Omega))$. This means that $T^n \longrightarrow T$ in $L^2(0,\tau;H^{3/4}(\Omega))$. Then by the continuity of the trace operator we have that $T^n_{|\partial\Omega} \longrightarrow T_{|\partial\Omega}$ in the space $L^2(0,\tau;L^2(\Omega))$. Consequently, extracting eventually a further subsequence, we have that $T^n_{|\partial\Omega} \longrightarrow T_{|\partial\Omega}$ in $L^2(\partial\Omega)$ for almost all $t \in (0,\tau)$. Using that the convergence in $L^2(\partial\Omega)$ implies also the convergence in $L^1(\partial\Omega)$ we conclude that

$$\int_{\Gamma(t)} T^n(t)dS = \int_{\partial\Omega} T^n(t)\mathcal{X}_{\Gamma(t)}dS \longrightarrow \int_{\partial\Omega} T(t)\mathcal{X}_{\Gamma(t)}dS = \int_{\Gamma(t)} T(t)dS\,.$$

In the same manner we can prove (possibly extracting a further subsequence) that $\bar{u}^n \longrightarrow \bar{u}$ for almost all $t \in (0,\tau)$. Now we are ready to pass to the limit. Let us fix $N > 0$. We choose $v = \sum_{k=1}^N d^k(t)v_k$ and $w = \sum_{k=1}^N \gamma^k(t)w_k$, where functions d^k and γ^k are smooth. Then from system (3.15) we obtain for each $\tau > 0$ and $n > N$

$$\begin{aligned}
&\varrho\int_0^\tau \langle \ddot{u}^n, v\rangle dt + \int_0^\tau\int_\Omega A\varepsilon(u^n)\varepsilon(v)dxdt + \delta\int_0^\tau\int_\Omega \varepsilon(\dot{u}^n)\varepsilon(v)dxdt \qquad (3.29a)\\
&\qquad = 3K\int_0^\tau\int_\Omega \beta(T^n)\operatorname{div} v dxdt + \int_0^\tau\int_{\Gamma(t)} f_2(q^n, q_\tau, \bar{u}^n, \bar{u}_\tau, \bar{T}^n)vdSdt\,,\\
&\varrho c_v\int_0^\tau \langle \dot{T}^n, w\rangle dt + \int_0^\tau\int_\Omega \kappa\nabla T^n\nabla w dxdt = -3K\alpha\int_0^\tau\int_\Omega T_0\operatorname{div} v\dot{u}^n w dxdt \qquad (3.29b)\\
&\qquad - \int_0^\tau\int_{\Gamma_0} \alpha_H(T^n - T_T)wdSdt + \int_0^\tau\int_{\Gamma(t)} f_1(q^n, q_\tau, \bar{u}^n, \bar{u}_\tau, \bar{T}^n)wdSdt\,.
\end{aligned}$$

Using the Lipschitz continuity of functions $f_1,\ f_2$ we conclude that

$$\begin{aligned}
&\varrho\int_0^\tau \langle \ddot{u}, v\rangle dt + \int_0^\tau\int_\Omega A\varepsilon(u)\varepsilon(v)dxdt + \delta\int_0^\tau\int_\Omega \varepsilon(\dot{u})\varepsilon(v)dxdt \qquad (3.30a)\\
&\qquad = 3K\int_0^\tau\int_\Omega \beta(T)\operatorname{div} v dxdt + \int_0^\tau\int_{\Gamma(t)} f_2(q, q_\tau, \bar{u}, \bar{u}_\tau, \bar{T})vdSdt\,,\\
&\varrho c_v\int_0^\tau \langle \dot{T}, w\rangle dt + \int_0^\tau\int_\Omega \kappa\nabla T\nabla w dxdt = -3K\alpha\int_0^\tau\int_\Omega T_0\operatorname{div} \dot{u} w dxdt \qquad (3.30b)\\
&\qquad - \alpha_H\int_0^\tau\int_{\Gamma_0} (T - T_T)wdSdt + \int_0^\tau\int_{\Gamma(t)} f_1(q, q_\tau, \bar{u}, \bar{u}_\tau, \bar{T})wdSdt
\end{aligned}$$

for all $v \in C^\infty(0,\tau;V_n)$, $w \in C^\infty(0,\tau;W_n)$. Using that these spaces are dense in $L^2(0,\tau;V)$, $L^2(0,\tau;H^1(\Omega))$ respectively we conclude (3.30) for all $v \in L^2(0,\tau;V)$, $w \in L^2(0,\tau;H^1(\Omega))$. Selecting $v = \varphi(t)v^*$, $w = \varphi(t)w^*$ where $\varphi \in C_0^\infty(0,\tau)$, $v^* \in V$, $w^* \in H^1(\Omega)$ we obtain that (u,T,q) satisfy in the weak sense two first equations of our problem. To go to the limit in (3.15c) we multiply (3.15c) by $\varphi \in C_0^\infty(0,\tau;\mathbb{R}^3)$ and integrate with respect to time

$$\begin{aligned}\int_0^\tau \ddot{q}^n \cdot \varphi dt + \int_0^\tau D\ddot{q}^n \cdot \varphi dt + \int_0^\tau Kq^n \cdot \varphi dt \\ = \int_0^\tau B(t,\bar{T}^n)(q^n - q_\tau^n - \bar{u}^n + u_\tau) \cdot \varphi dt\,.\end{aligned} \tag{3.31}$$

From the strong convergence $\bar{T}^n \longrightarrow \bar{T}$ in $L^2(0,\tau)$ we have that $B(\cdot,\bar{T}^n) \longrightarrow B(\cdot,\bar{T})$ in $L^2(0,\tau)$. Consequently, passing to the limit we obtain

$$\int_0^\tau \ddot{q} \cdot \varphi dt + \int_0^\tau D\dot{q} \cdot \varphi dt + \int_0^\tau Kq \cdot \varphi dt = \int_0^\tau B(t,T)(q - q_\tau - \bar{u} + u_\tau)\varphi dt\,.$$

Using that φ is chosen arbitrary we conclude that for almost all $t \in (0,\tau)$

$$\ddot{q} + D\dot{q} + Kq = B(\cdot,T)(q - q_\tau - \bar{u} + u_\tau)\,.$$

To end the proof we need to show that the initial conditions are satisfied. $q^n \longrightarrow q$ in $L^\infty(0,\tau)$ hence in $L^\infty(-\tau,\tau)$ also. Consequently, $q(s) = w(s)$ for $s \in [-\tau,0]$. Let us write (3.29b) in the form

$$\varrho c_v \int_0^\tau \langle \dot{T}^n, w\rangle dt = RHS \tag{3.32}$$

where RHS is the sum of the right-hand side of (3.29b) and the term

$$-\int_0^\tau \int_\Omega \kappa \nabla T^n \nabla w dx dt\,.$$

Let us choose w with $w(\tau) = 0$. Then integrating by parts on the left-hand side of (3.32) we have

$$-\varrho c_v \int_0^\tau \langle T^n, \dot{w}\rangle dt - (T^n(0), w(0)) = RHS\,. \tag{3.33}$$

Then going to the limit in (3.33) and using that $C^\infty([0,\tau];W_n)$ is dense in $C^1([0,\tau];H^1(\Omega))$ we obtain that

$$-\varrho c_v \int_0^\tau \langle T, \dot{w}\rangle dt - (T_0, w(0)) = RHS \tag{3.34}$$

for all $w \in C^1([0,\tau];H^1(\Omega))$ with $w(\tau) = 0$. Writing (3.30b) in the form

$$\varrho c_v \int_0^\tau \langle \dot{T}, w\rangle dt = RHS \tag{3.35}$$

and integrating by parts with respect to t, selecting again $w \in C^1([0,\tau];H^1(\Omega))$ with $w(\tau) = 0$ we have

$$-\varrho c_v \int_0^\tau \langle T, \dot{w}\rangle dt - (T(0), w(0)) = RHS\,. \tag{3.36}$$

Comparing (3.34) and (3.36) we have that

$$(T(0)w(0)) = (T_0, w(0)) \quad \text{for all } \; w \in C^1([0,\tau]; H^1(\Omega)) \quad \text{with } \; w(\tau) = 0\,.$$

Consequently, we have $T(0) = T_0$. (Note that $\dot{T} \in L^2(0,\tau;(H^1(\Omega))^*)$ and $T \in L^2(0,\tau; H^1(\Omega))$ implies $T \in C([0,\tau]; L^2(\Omega))$ whence $T(0)$ is well defined.) The proof for $u(0) = u_0$ and $\dot{u}(0) = u_1$ is similar and therefore omitted. ∎

Finally, we show that weak solutions with the regularity obtained in Theorem 3.1 are unique.

Theorem 3.2 *Let us fix $\tau > 0$. Then weak solutions with the regularity from Theorem 3.1 satisfying the same initial conditions are unique.*

Proof: Let (u^1, T^1, q^1) and (u^2, T^2, q^2) be two weak solutions of the problem (3.10), (3.13), (3.14) satisfying the initial conditions (3.5) and (3.11). Let us denote by $(u, T, q) = (u^1 - u^2, T^1 - T^2, q^1 - q^2)$. Then these functions satisfy

$$\begin{aligned}\langle \varrho\ddot{u}, v\rangle + \int_\Omega A\varepsilon(u)\varepsilon(v)dx + \delta\int_\Omega \varepsilon(\dot{u})\varepsilon(v)dx = 3K\alpha\int_\Omega T\,\mathrm{div}\, v dx\\ + \int_{\Gamma(t)} \big(f_2(q^1, q_\tau, \bar{u}^1, \bar{u}_\tau, \bar{T}^1) - f_2(q^2, q_\tau, \bar{u}^2, \bar{u}_\tau, \bar{T}^2)\big) v dS\\ \forall v \in V \quad \text{and a.e. } \; t \in (0,\tau)\,,\end{aligned} \tag{3.37}$$

$$\begin{aligned}\langle \varrho c_v\dot{T}, w\rangle + \kappa\int_\Omega \nabla T\nabla w = -3K\alpha\int_\Omega T_0\,\mathrm{div}\,\dot{u} w dx - \int_{\Gamma_0}\alpha_H(T - T_T) w dS\\ + \int_{\Gamma(t)} \big(f_1(q^1, q_\tau, \bar{u}^1, \bar{u}_\tau, \bar{T}^1) - f_1(q^2, q_\tau, \bar{u}^2, \bar{u}_\tau, \bar{T}^2)\big) w dS\\ \forall w \in H^1(\Omega) \quad \text{and a.e. } \; t \in (0,\tau)\,,\end{aligned} \tag{3.38}$$

$$\ddot{q} + D\dot{q} + Kq = B(t, \bar{T}^1)(q - \bar{u}) + (B(t, \bar{T}^1) - B(t, \bar{T}^2))(q^2 - q_\tau - \bar{u}^2 + \bar{u}_\tau)\,. \tag{3.39}$$

Multiplying the last equality by $\dot{q}$ and exploiting the fact that on the time interval $(0,\tau)$ functions q^1, q^1_τ, q^2, q^2_τ and $\bar{u}^1$, $\bar{u}^2$ are bounded, we easily obtain the existence of a positive constant $M(\tau)$ such that

$$\begin{aligned}\frac{1}{2}|\dot{q}|^2 + \int_0^t D\dot{q}\cdot\dot{q}d\tau + \frac{1}{2}Kq\cdot q \le M(\tau)\bigg(\int_0^t |B(t,\bar{T}^1)|^2|\dot{q}|^2 d\tau + \int_0^t |\bar{T}|^2 d\tau\\ + \int_0^t |q|^2 d\tau + \int_0^t |\bar{u}|^2 d\tau\bigg)\,.\end{aligned} \tag{3.40}$$

By the Gronwall's inequality we conclude that for all $t \in (0,\tau)$

$$|\dot{q}|^2 + |q|^2 \le \bar{M}(\tau)\bigg(\int_0^\tau |\bar{u}|^2 d\tau + \int_0^\tau |\bar{T}|^2 d\tau\bigg)\,. \tag{3.41}$$

(Note that $\int_0^\tau |B(t,\bar{T}^1)|^2 d\tau$ is bounded by a constant depending on τ only.)

Next we insert into (3.37) $v = \dot{u}(t)$ and into (3.38) $w = T(t)$ as test functions. Since f_1 and f_2 are globally Lipschitz, we obtain

$$\begin{aligned}\varrho\frac{d}{dt}\frac{1}{2}\|\dot{u}\|^2_{L^2(\Omega)} + \frac{d}{dt}\frac{1}{2}\int_\Omega A\varepsilon(u)\varepsilon(u)dx + \delta\int_\Omega|\varepsilon(\dot{u})|^2dx \\ \leq 3\alpha K\int_\Omega|T|\,|\operatorname{div}\dot{u}|dx + L_2\int_{\Gamma(t)}(|q|+|\bar{u}|+|\bar{T}|)|\dot{u}|dS\end{aligned} \tag{3.42}$$

$$\begin{aligned}\varrho c_v\frac{d}{dt}\frac{1}{2}\|T\|^2_{L^2(\Omega)} + \kappa\|\nabla T\|^2_{L^2(\Omega)} \leq 3K\alpha\sup_\Omega|T_0|\int_\Omega|\operatorname{div}\dot{u}|\,|T|dx \\ + \int_{\Gamma(t)}\alpha_H|T|T_T dS + L_1\int_{\Gamma(t)}(|q|+|\bar{u}|+|\bar{T}|)|T|dS\end{aligned} \tag{3.43}$$

where by L_i we have denoted the Lipschitz constant of f_i, $i = 1, 2$. Estimating the first integral in (3.42) and (3.43) in the same manner as in (3.20) and using (3.41) and (3.24) we arrive at the inequality

$$\begin{aligned}\varrho\frac{1}{2}\|\dot{u}\|^2_{L^2(\Omega)} + \frac{1}{2}\int_\Omega A\varepsilon(u)\varepsilon(u)dx + \frac{\delta}{2}\int_0^t\int_\Omega|\varepsilon(\dot{u}|^2dx \\ + \varrho c_v\frac{1}{2}\|T\|^2_{L^2(\Omega)} + \frac{\kappa}{2}\int_0^t\|\nabla T\|^2_{L^2(\Omega)}dx \leq M(\tau)\Big[\int_0^t\|\varepsilon(u)\|^2_{L^2(\Omega)}d\tau \\ + \int_0^t\|T\|^2_{L^2(\Omega)}d\tau\Big] \quad \text{where } M(\tau) > 0 \quad \text{is a constant.}\end{aligned}$$

Again applying Gronwall's inequality we have that $u = 0$, $T = 0$ and consequently $q = 0$. ∎

Remark 3.3 *Applying the method of steps as explained in this beginning of this section we can extend the existence and uniqueness result to the complete time domain* $[0, t_E]$.

4 Numerical simulations

4.1 The Algorithm

4.1.1 The outer iteration

To avoid technicalities, in the sequel we focus on milling processes where the pitch angle is smaller than the difference between exit and entry angle, which means that only one tooth is in cut at a time. We use the method of steps as explained in Section 3. However, in addition we now allow for non-zero feeding velocity of the cutter. Therefore, we have to account for changing workpiece geometry due to material removal. The first stage in each iteration is to compute the new workpiece geometry Ω_l. Next, the system (3.15a)–(3.15c) is solved on the space-time domain $\Omega_l \times (l\tau, (l+1)\tau)$. In the following subsections we explain important features of the method.

4.1.2 Computation of mean values $\bar{u}$ and $\bar{T}$

We define the theoretical tooth path, which is the fictitious manifold created by the points on the cutting edge during one tooth period, if we neglect the displacement of the cutter and the deformation of the workpiece. For $s \in [0, \tau]$ and $\zeta \in [0, a_p]$ we parametrise the respective manifold with the following expression:

$$\begin{aligned} P_t(s,\zeta) = \frac{D}{2}&(\cos\psi(s), \sin\psi(s), 0)^T \\ &+ (X_0 - \left(N_e(t) + \frac{s}{\tau}\right) f_z, Y_0, Z_0 + \zeta)^T, \\ \text{with} \qquad &\psi(s) = 2\pi s + \varphi_S. \end{aligned} \tag{4.1}$$

The number of elapsed tooth periods is defined as $N_e(t) = \text{int}(t/\tau)$, with int(.) being the integer part of a real number. The vector $(X_0, Y_0, Z_0)^T$ represents the position of the cutter tip with respect to the workpiece reference frame at $t = 0$. Using the above parametrisation we define the cutting zone

$$\Gamma(t) = \{P_t(s,\zeta) \mid \ 2|\bar{s}(t) - s| \leq \Delta s \text{ and } \zeta \in [0, a_p]\}, \tag{4.2}$$

with $\bar{s} = t - N_e(t)$. Δs is a parameter depending on the cutting conditions. We compute the mean value $\bar{a}(t) = a^*(t)|\Gamma(t)|^{-1}$ of an arbitrary field $a(t, x)$ with the integral over the cutting zone:

$$a^*(t) = \int_0^{a_p} \int_{\bar{s}(t)-\Delta s/2}^{\bar{s}(t)+\Delta s/2} a\left(t, P_t(s,\zeta)\right) \ |\partial_s P_t \times \partial_\zeta P_t| \ ds \ d\zeta. \tag{4.3}$$

Note that we get $a^*(t) = |\Gamma(t)|$ for $a(t, x) = 1$.

4.1.3 Geometry update

During one tooth period, the cutter removes a certain amount of material from the workpiece. We simulate this effect by a modification of the workpiece shape after each tooth period. We assume that the workpiece changes according to the theoretical tooth path given by the static chip thickness (i.e. the first term in (2.25)). After the tooth period $[(l-1)\tau, l\tau]$ with workpiece domain Ω_{l-1}, as shown for instance in Figure 1, we have to compute a new domain Ω_l representing the workpiece shape during the next tooth period, i.e. $t \in [l\tau, (l+1)\tau]$.

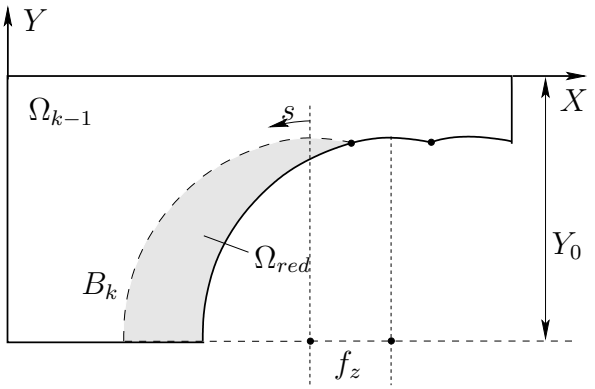

Figure 3: Reduction of workpiece domain.

The first step is the calculation of the volume Ω_{red} that shall be removed from the workpiece. To this end we introduce a manifold $B_l \subset \mathbb{R}^3$, defined by the given parametrisation $P_t(s,\zeta) : \mathbb{R} \times \mathbb{R} \to \mathbb{R}^3$, (cf. (4.1))

$$B_l = \{P_{l\tau}(s,\zeta) | s \in [s_-, \tau], \zeta \in [0, a_p]\}, \tag{4.4}$$

where the coordinate $s_- \in [-\tau, 0]$ is the biggest non positive solution of the equation:

$$\sin\left[\omega\big(s + \tau - \frac{D\tau}{f_z}\cos[\omega s + \varphi_{st}]\big) + \varphi_{st}\right] = \sin[\omega s + \varphi_{st}], \tag{4.5}$$

which may be derived from the condition that two successive arcs must have at least one common intersection point.The domain Ω_{red} that should be removed form the workpiece reads:

$$\begin{aligned}\Omega_{red}(t) = \{r \in \Omega_{n-1} | \exists R \in B(t), \text{ such that} \\ r_x = R_x \wedge Y_0 \leq r_y \leq R_y \wedge r_z = R_z\}.\end{aligned} \tag{4.6}$$

With $\Omega_{red}(t)$ we may now define the new workpiece domain:

$$\Omega_l = \Omega_{l-1} \setminus \Omega_{red}. \tag{4.7}$$

With a given starting geometry Ω_0 we create after each tooth period a new workpiece shape using the algorithm described above. Afterwards we interpolate the solution of the space discrete problem from the old grid to the new one and we proceed with the time integration as explained in the following section.

4.1.4 Time integration algorithm

In this section we construct a time integration algorithm for the system (3.15a),(3.15b) and (3.15c) considering an arbitrary tooth period. Using linear finite elements in space we obtain the following system of ordinary differential equations with delay:

$$\begin{aligned}M_h\ddot{u}_h + D_h\dot{u}_h + K_h u_h &= +C_h T_h + F_h\Big(t, q(t), q(t-\tau), \bar{u}_h(t), \bar{u}_h(t-\tau), \bar{T}_h(t)\Big), \\ m_h\dot{T}_h + \kappa_h T_h &= -c_h\dot{u}_h + f_h\Big(t, q(t), q(t-\tau), \bar{u}_h(t), \bar{u}_h(t-\tau), \bar{T}_h(t)\Big), \\ \ddot{q}(t) + D\dot{q}(t) + Kq(t) &= B(t, \bar{T}_h(t))(q(t) - q(t-\tau) - \bar{u}_h(t) + \bar{u}_h(t-\tau)).\end{aligned}$$

The system is solved numerically in the interval $[l\tau, (l+1)\tau]$ by an incremental decoupling using an implicit Newmark scheme (cf. Hughes [8]) for the momentum balance, an implicit Euler scheme for the energy balance and a Runge-Kutta 54 algorithm (cf. Deuflhard et al. [3]) to solve the remaining dde.

4.2 Simulation results

4.2.1 Data

The system of equations has unstable and stable solutions depending on the parameters rotation speed n, number of teeth N_z, axial depth of cut a_p and radial depth of cut. For the simulations we fix the cutting parameters $f_z = 0.2\ mm$, $N_z = 4$, $\varphi_s = \pi/2$, $\varphi_E = \pi$, $D = 15\ mm$ and $n = 7500\ rpm$. We only modify the parameter a_p and the workpiece geometry to choose between stable and unstable solutions. Tables 1-3 depict the values of the various parameters used in the simulations.

	λ	μ	α	ϱ	c_v	κ
value	51.084e9 Pa	26.316e9 Pa	23e-6 K^{-1}	2700 $\frac{kg}{m^3}$	900 $\frac{J}{kg\ K}$	160 $\frac{J}{m\ sec\ K}$

Table 1: Material parameters for the aluminium workpiece.

	m_c	ζ_1	ζ_2	ω_1	ω_2
value	0.3993 kg	1.1%	1.1%	922 Hz	922 Hz

Table 2: Material parameters for the cutter dynamics.

	$\hat{K}_R$	$\hat{K}_T$	β_{Fr2}	β_{Sh2}	β_{Ch}	c_R	c_T	l_{c2}	α_R
value	200 $\frac{N}{mm^2}$	600$\frac{N}{mm^2}$	50%	90%	15%	0.0582	0.0671	0.1mm	20°

Table 3: Material parameters for the cutting forces and the heat source.

In each simulation run we set $t_e = 50\tau$, i.e., for the choice of n and N_z, $t_e = 0.1\ sec$.

4.2.2 Stable situation

For the first example the axial depth of cut is $a_p = 1\ mm$ and we have chosen a rather rigid workpiece geometry. The edge lengths of the workpiece are $l_x = 25\ mm$, $l_y = 15\ mm$, $l_z = 10\ mm$ and the initial position of the cutter tip is $X_0 = 25\ mm$, $Y_0 = 8\ mm$, $Z_0 = 9\ mm$. In Figure 5, we see the results of the first simulation run. Since the uncut chip thickness converges to a stationary state, we identify this milling process as stable. Moreover, we observe an increase of the workpiece temperature during the simulation. The temperature at the beginning of each tooth period rises form the initial temperature $T_0 = 293.17K$ to approximately $300K$.

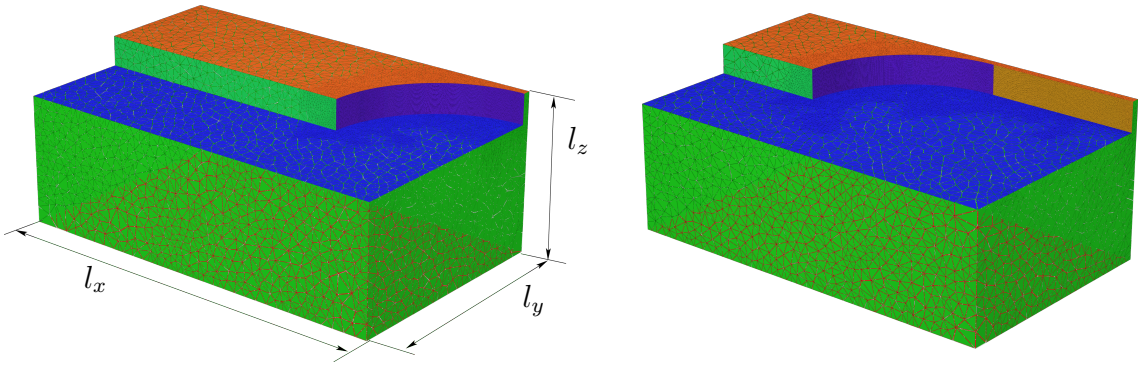

Figure 4: The initial and final workpiece grid.

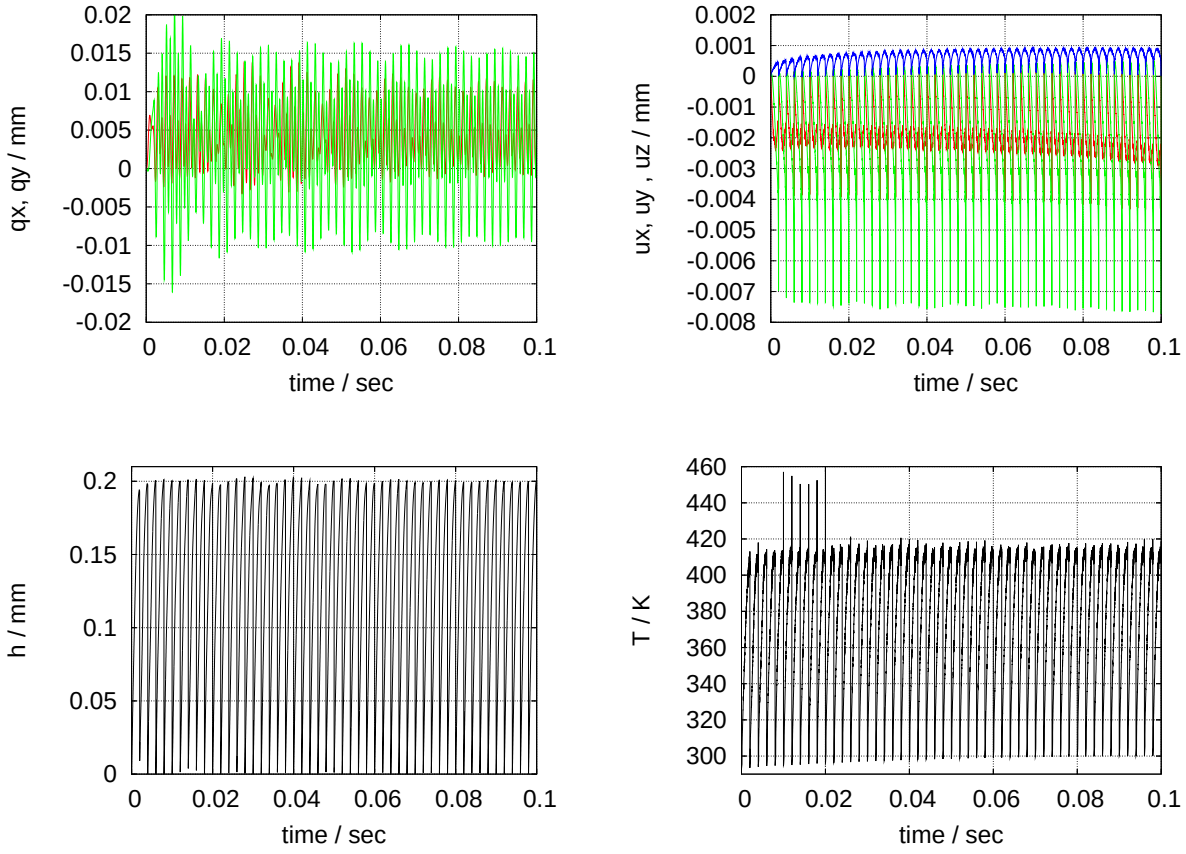

Figure 5: Cutter vibrations, mean workpiece deformations, uncut chip thickness and mean temperature at the cutting edge (x-, y-, z- component printed in red, green, blue, respectively).

However, the induced deformations do not interfere with the stable cutting conditions. The workpiece deformations are one order of magnitude smaller than the cutter vibrations. We hence conclude that in the present example the dynamic characteristics of the harmonic oscillator dominates the stability of the entire system.

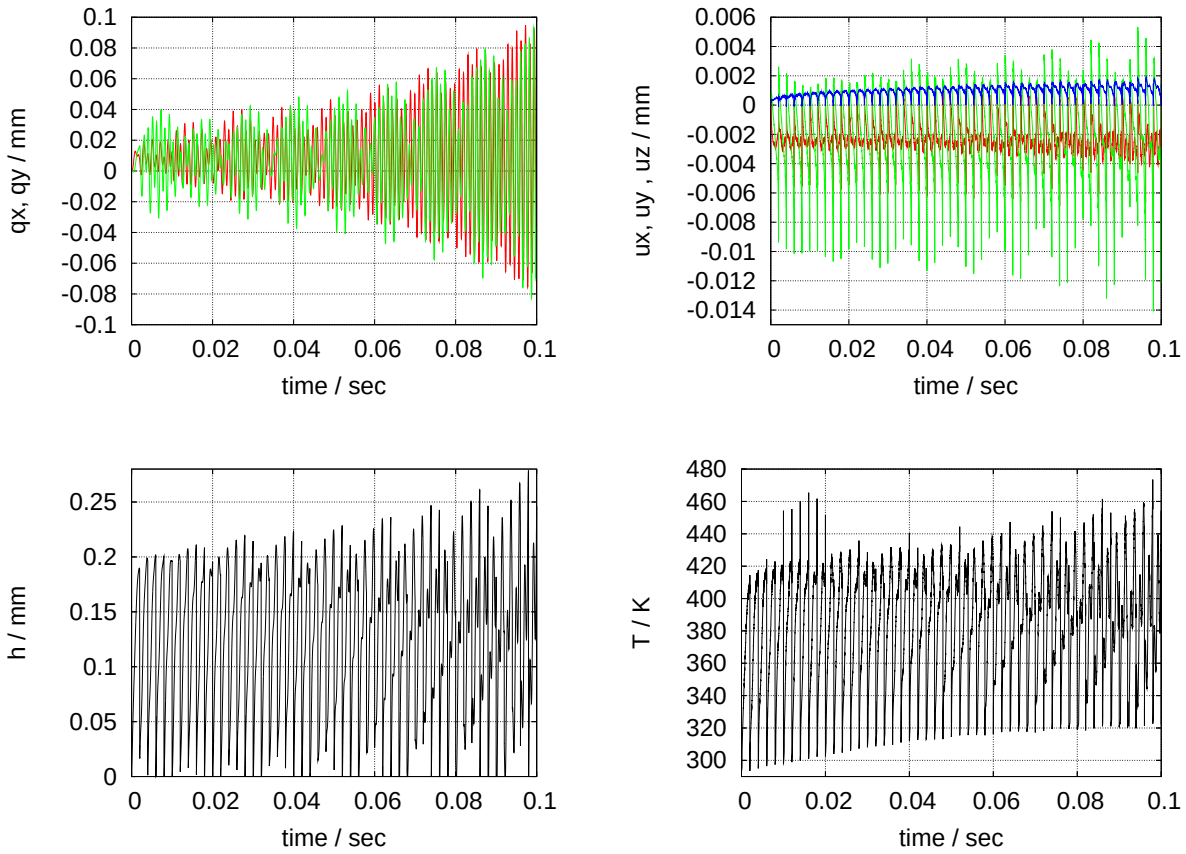

Figure 6: Cutter vibrations, mean workpiece deformations, uncut chip thickness and mean temperature at the cutting edge (x-, y-, z- component printed in red, green, blue, respectively).

4.2.3 Cutter induces the loss of stability

In this example we choose the same workpiece shape as in the preceeding example (cf. Figure 4). The only difference is that we increased the axial depth of cut $a_p = 1.9\ mm$. The corresponding initial position of the cutter is now $X_0 = 25\ mm$, $Y_0 = 8\ mm$, $Z_0 = 8.1\ mm$. Figure 6 shows the simulation results. A comparison to the results given in Figure 5 clearly indicates the instability of the current process. The uncut chip thickness doesn't converge to the stationary solution but increases during the simulation run. At the end the maximum of the uncut chip thickness is significantly bigger than the feed. These observations are confirmed by the workpiece deformations. The workpiece deformations reflect the evolution of the chip thickness and they hence don't converge to a stationary state. Due to the increase of the uncut chip thickness h, the cutting forces grow and thus the heat generated by the process. This is directly confirmed by the workpiece temperature that rises during the simulation faster than in the previous case. While the temperature is at the beginning of the first tooth period equal to the initial temperature $T_0 = 293.17\ K$, we observe at the beginning of the last tooth period a temperature of $320\ K$. However, all these effects are induced by the vibrations of the harmonic oscillator. Here we clearly notice the divergence of the vibration amplitude which is an indicator for the loss of stability. This effect is also observed in case of uncoupled systems, where the

increase of the depth of cut induces the loss of stability (cf. Altintas et al. [2]).

4.2.4 Workpiece induces the loss of stability

For the next example the axial depth of cut is $a_p = 1\ mm$ and we have chosen a workpiece geometry as depicted in Figure 7. The workpiece has a very low stiffness in y-direction.

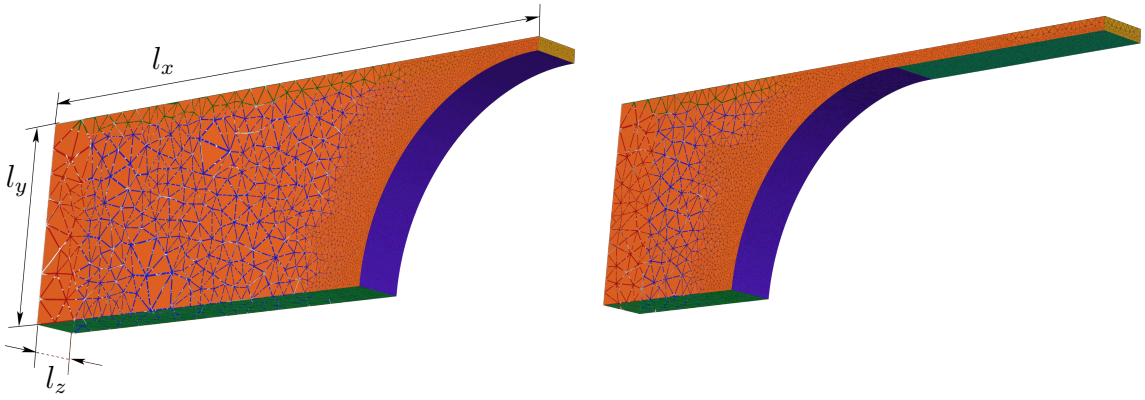

Figure 7: Initial and final workpiece grid.

The edge lengths of the workpiece are $l_x = 25\ mm$, $l_y = 8\ mm$, $l_z = a_p = 1\ mm$ and the initial position of the cutter is $X_0 = 25\ mm$, $Y_0 = 8\ mm$, $Z_0 = 0\ mm$. Note that we fixed the workpiece on the part of the boundary where coordinate $X = 0\ mm$. Due to the special shape of the workpiece, the process of considered in example 4.2.2 becomes unstable. The magnitude of the workpiece vibrations rise until $t = 0.04\ sec$. Then after a short decay they rise again and finally for $t > 0.06\ sec$ they decrease until the end of the simulation run. Note that from a physical point of view the simulations are not meaningful for $t > 3\tau$, say. Since the workpiece deformation affects the cutting forces via the uncut chip thickness, the cutting heat attains very high values inducing the huge temperatures at the cutting edge. However, we may clearly identify the unstable cutting conditions from the computed uncut chip thickness. Due to the nonlinearities in the model (recall that we use $\max(h, 0)$ to compute the cutting forces) the amplitudes remain finite and do not rise until the end of the simulation run. A possible action to stabilise this process would be the reduction of the radial depth of cut, i.e., the reduction of the difference of φ_s and φ_e, which reduces on the one hand the cutting forces and the increases on the other hand the stiffness of the workpiece.

4.2.5 Workpiece and cutter induce the loss of stability

For this last example the axial depth of cut is $a_p = 1.9\ mm$ corresponding to the unstable situation of example 4.2.3. Additionally we have chosen the non stiff workpiece geometry of example 4.2.4. The edge lengths of the workpiece are $l_x = 25\ mm$, $l_y = 8\ mm$, $l_z = a_p = 1.9\ mm$ and the initial position of the cutter tip is $X_0 = 25\ mm$, $Y_0 = 8\ mm$, $Z_0 = 0\ mm$. As before, we fixed the workpiece on the $X = 0\ mm$ plane. The current example is very similar to example 4.2.4. However, in comparison to the previous example we increased the thickness of the workpiece by a factor 1.9, which also affects the workpiece stiffness.

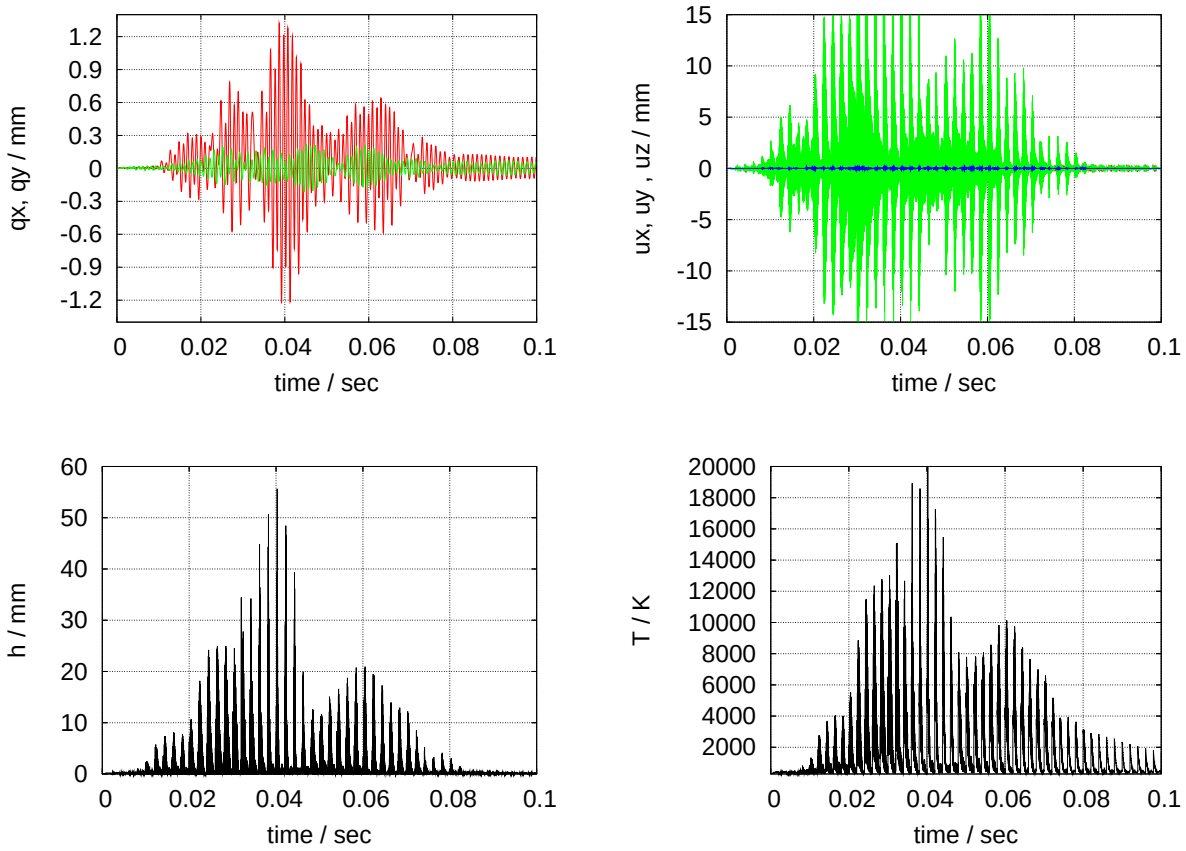

Figure 8: Cutter vibrations, mean workpiece deformations, uncut chip thickness and mean temperature at the cutting edge (x-, y-, z- component printed in red, green, blue, respectively).

Thus, the maximum of the workpiece deformation and the maximum of the temperature are much smaller than the respective values in case 4.2.4. Another observation is that the cutter mainly vibrates in x-direction while the workpiece shows the most important oscillations in y-direction. In this example both parts workpiece and cutter contribute to the unstability of the process. For $t < 0.07$ *sec* the workpiece oscillations dominate the uncut chip thickness and for $t > 0.07$ *sec* with the increasing stiffness of the workpiece the effect of the large cutter vibrations becomes more important. As in the previous example, the results for $t > 3\tau$, say, are no longer physically meaningful. Again, a possible stabilisation would be to decrease the radial depth of cut.

5 Conclusions

The goal of this paper was to enhance existing models of the milling process to allow for the consideration of the workpiece influence. The simulations in Section 4 clearly show that the model is capable of reproducing instability effects due to a lack of workpiece stiffness.

The results are promising and open up various directions for future research. From mathematical point of view the inclusion of a refined multibody system to describe the machine

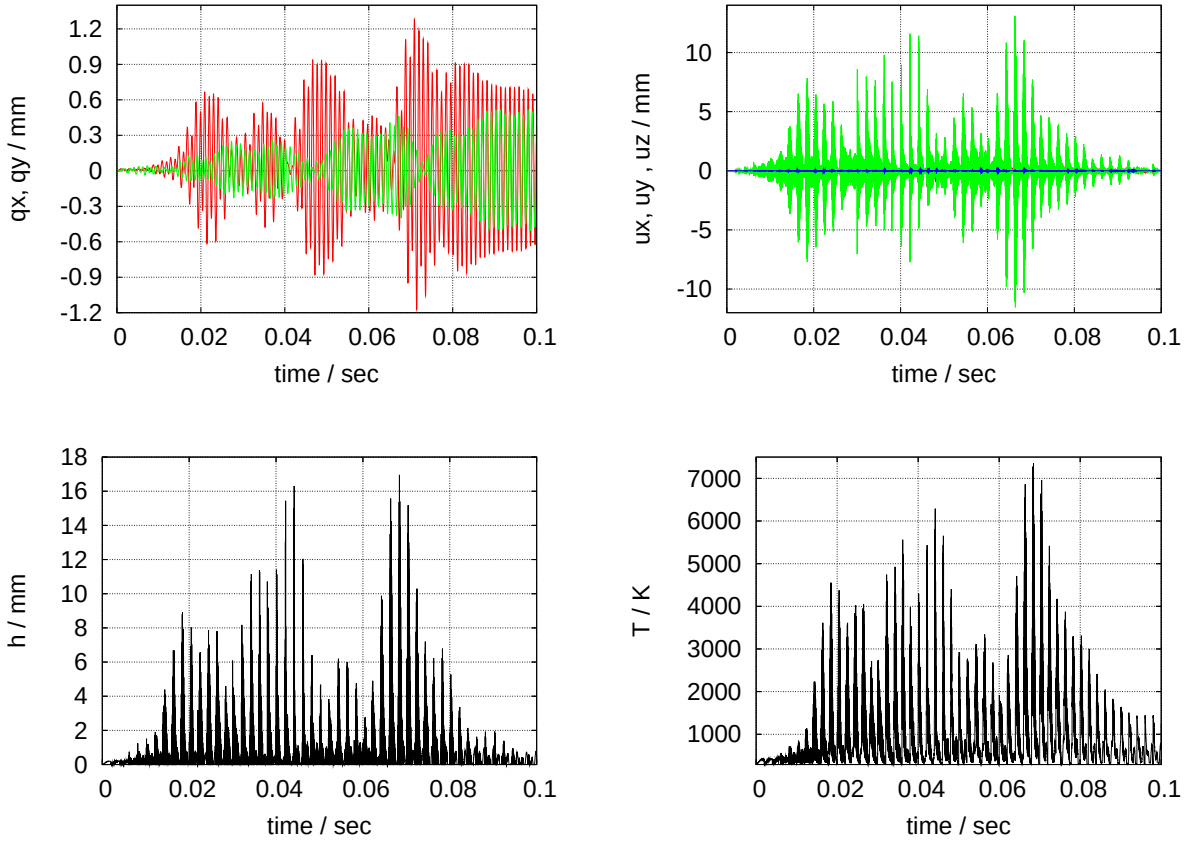

Figure 9: Cutter vibrations, mean workpiece deformations, uncut chip thickness and mean temperature at the cutting edge (x-, y-, z- component printed in red, green, blue, respectively).

dynamics would pose no further difficulty. Then a challenging task would be to investigate the stability of milling processes with respect to variations in the machine design.

Another interesting task would be the coupling of the classical DDE-model of the cutter with a simplified workpiece model, e.g., a beam. This situation should allow for a stability analysis along the lines of the bifurcation results mentioned in Section 1.

Finally, from application point of view an efficient numerical tool for the systematic derivation of stability diagrams would be most desirable. This would require the numerical solution of a large parameter-dependent Hamiltonian eigenvalue problem and is subject to further research.

References

[1] Y. Altintas, *Manufacturing automation*, Cambridge University Press, 2000.

[2] Y. Altintas and M. Weck, *Chatter stability of metal cutting and grinding*, Annals of the CIRP **53/2** (2004).

[3] P. Deuflhard and F. Bornemann, *Scientific computing with ordinary differential equations*, Springer, Berlin Heidelberg, 2002.

[4] H. Ernst and M. E. Merchant, *Chip formation, friction and high quality machined surfaces*, Trans. ASM (1941).

[5] R. P. H. Faassen, N. van de Wouw, J.A.J. Oosterling, and H. Nijmeijer, *Prediction of regenerative chatter by modelling and analysis of high-speed milling*, International Journal of Machine Tools and Manufacture (2003).

[6] A. G. Harris, *An investigation to derive a method of predicting the contribution of tool flank wear to tool forces in orthorgonal machining*, Tech. Report ISSN 0156-3068, University of New South Wales, 1981.

[7] P. Haupt, *Continuum mechanics and theory of materials*, Advanced texts in physics, Springer, Berlin Heidelberg, 2000.

[8] T. J. R. Hughes, *The finite element method*, Dover Publications, New York, 2000.

[9] T. Insperger and G. Stépán, *Updated semi-discretization method for periodic delay-differential equations with discrete delay*, International Journal for Numerical Methods in Engineering (2004).

[10] E. H. Lee and B. W. Schafer, *The theory of plasticity applied to a problem of machining*, Journal of Applied Mechanics (1951).

[11] Bernhard Müller, *Thermische analyse des zerspanens metallischer werkstoffe bei hohen schnittgeschwindigkeiten*, Ph.D. thesis, Rheinisch-Westflische Technische Hochschule Aachen, 2004.

[12] T. Roubiček, *Nonlinear partial differential equations with applications*, Internat. Ser. Numer. Math., no. 139, Birkhäuser, Basel, 2005.

[13] M. Weck and K. Teipel, *Dynamisches Verhalten spanender Werkzeugmaschinen*, Springer Berlin Heidelberg New York, 1977.